International Journal of Solids and Structures 49 (2012) 3754–3761

Contents lists available at SciVerse ScienceDirect

International Journal of Solids and Structures

journal homepage: www.elsevier.com/locate/ijsolstr

Electromechanical and dynamic analyses of tunable dielectric elastomer resonator

Tiefeng Li, Shaoxing Qu, Wei Yang *

Department of Engineering Mechanics, Zhejiang University, Hangzhou 310027, China
Soft Matter Research Center (SMRC), Zhejiang University, Hangzhou 310027, China

ARTICLE INFO

Article history:
Received 7 January 2012
Received in revised form 7 July 2012
Available online 17 August 2012

Keywords:
Dielectric elastomer
Electromechanical
Dynamic
Instability

ABSTRACT

When used as resonators, dielectric elastomers are subjected to high frequencies and nonlinear oscillation. The present study is focused on a dielectric elastomer resonator whose dielectric membrane is subject to combined loads of tensile forces and voltages. When the loads are static, the resonator may reach a state of equilibrium. The stability and the natural frequency of the resonator with small-amplitude oscillation around the equilibrium state are analyzed. When a periodic voltage is applied, the device resonates at multiple frequencies of excitation. Pre-stretches and applied static voltages tune the natural frequency and modify the dynamic behavior of the resonator. The membrane may suffer loss of tension and electromechanical instability, causing the failure of the resonator. Safe operation range is identified for failure prevention while actuating the resonator.

1. Introduction

Dielectric elastomer (DE) consists of a soft elastomeric membrane sandwiched within two compliant electrodes on both sides. When a voltage is applied through the thickness, the DE membrane contracts in thickness and expands in area. Transducers made of DE possess excellent deformability, flexibility, affordability, and chemical and biological compatibility (Pelrine et al., 2000; Wissler and Mazza, 2005a,b; Carpi et al., 2008, 2010). Recently, DE transducers have been widely used as resonators, artificial muscles, adaptive optical elements, and programmable haptic surfaces (Bar-Cohen, 2002; Xia et al., 2005; Anderson et al., 2010; Mckay et al., 2010).

Most of the previous studies on DEs were focused on quasi-static deformation, with the effect of inertia neglected. In recent applications such as resonators, DEs can operate at a frequency as high as 50 kHz (Bonwit et al., 2006) in many applications and function as vibration sources. DE resonators exhibit promising advantages over conventional resonators since their natural frequencies can be set by structural parameters during fabrication and can be actively tuned by the applied static voltage. Researchers have designed DE resonators with different configurations. In a large-strain, high-frequency application, the elastomer membrane undergoes nonlinear oscillation. The dynamic behavior of a DE membrane resonator under voltages and pressures has been investigated (Mockensturm and Goulbourne, 2006; Fox, 2007; Fox and Goulbourne, 2008, 2009). Dubois et al. (2008) demonstrated the active tuning of resonant frequencies by applying voltage on a circular membrane resonator. Zhu et al. (2010a) and Yong et al. (2011) theoretically studied the dynamic behavior of DE membrane resonators. Feng et al. (2011) studied the oscillation of a DE-based micro-beam resonator and predicted the performance of the device against the Q-factor and the resonant frequency shift ratio. Interesting phenomena under electromechanical loads have been reported in DE actuators. Kollosche et al. (2012) investigated the 'pure-shear' DE actuators and observed that the voltage-deformation transition, the electromechanical instability and the loss of tension may occur during actuation, while the pre-stretches significantly alter the behavior of actuators. Keplinger et al. (2011) and Li et al. (submitted for publication) investigated a DE-based membrane inflation actuator and showed that the voltage-deformation response of the actuator was dictated by the mechanical loading paths. Explored also are the modes of failure that limit the performance of DE transducers (Wissler and Mazza, 2005a,b; Plante and Dubowsky, 2006, 2007; Carpi et al., 2010). Artificial Muscle Inc. (AMI) has fabricated a resonator recently, named Reflex™ HIC Slide Actuator HIC-512 (Biggs and Hitchcock, 2010). The resonator consists of soft dielectric membranes, a rigid frame and mass bars. The dynamic performances, such as strokes and acceleration responses, of the resonator with different input frequencies were examined in experiments. However, the pre-stretch effect and loading paths effect on actuation, loss of tension, electromechanical instability, and active tuning of the resonate frequency have yet to be studied for this DE-based resonator.

The aim of this paper is to develop an analytical model for the tunable dielectric elastomer resonator, with specific configuration referred to the Reflex™ HIC Slide Actuator HIC-512. The attention

* Corresponding author at: Department of Engineering Mechanics, Zhejiang University, Hangzhou 310027, China.
E-mail address: yangw@zju.edu.cn (W. Yang).

0020-7683/$ - see front matter © 2012 Elsevier Ltd. All rights reserved.
http://dx.doi.org/10.1016/j.ijsolstr.2012.08.006

is focused on the pre-stretch and loading paths effects on actuation, as well as loss of tension, electromechanical instability, and active tuning of the resonate frequency. The work is presented as follows. Section 2 derives the equation of motion using the method of virtual work. Section 3 describes the state of equilibrium under static loads. Section 4 studies the small oscillation around the equilibrium state, as well as the tuning of the natural frequency of the resonator by pre-stretches and static applied voltages. Section 5 studies the parametric excitation with sinusoidal voltage.

2. Equation of motion

When an AC voltage is applied, the resonator oscillates around the state of equilibrium. The small-amplitude oscillation is governed by the equation of motion. To analyze the electromechanical behavior of the DE resonator, we derive the equation of motion under oscillation considering the inertia effect. Fig. 1 shows the schematics of the resonator. Fig. 1a displays a DE membrane of thickness H, with length L_1 in the 1-direction and L_2 in the 2-direction in a non-deformed state. The membrane is pre-stretched with the stretch λ_{1p} in the 1-direction and λ_{2p} in the 2-direction, as illustrated in Fig. 1b. The membrane is then attached to a rigid frame to maintain the pre-stretch. Two rigid mass bars with lumped mass m sandwich the dielectric elastomer membrane and divide it into two parts, marked as membrane A and membrane B. As shown in Fig. 1a, L_{1A} and L_{1B} are the original lengths along the 1-direction of membranes A and B in the undeformed state, with $L_{1A} + L_{1B} = L_1$. After the pre-stretch, membrane A is deformed to $\lambda_{1p}L_{1A}$ along the 1-direction and is coated on both surfaces with compliant electrodes as the active part. The passive part, membrane B, is deformed to $\lambda_{1p}L_{1B}$ in the 1-direction. In the actuated state, a voltage Φ_A is applied to the two electrodes of membrane A, as depicted in Fig. 1c. Membranes A and B have the deformed lengths $L_{1A}\,\lambda_{1A}$ and $L_{1B}\lambda_{1B}$ in the 1-direction, and $L_2\lambda_{2A}$ and $L_2\lambda_{2B}$ in the 2-direction. Here λ_{1A}, λ_{1B}, λ_{2A}, and λ_{2B} denote the stretches. Because the DE membranes are incompressible, membranes A and B have the deformed thicknesses $H/(\lambda_{1A}\lambda_{2A})$ and $H/(\lambda_{1B}\lambda_{2B})$. Electrons flow from one electrode of membrane A to the other and the two electrodes gain charges $+Q_A$ and $-Q_A$. Viewing membrane A as a parallel capacitor, one may calculate the charge on the electrode as

$$Q_A = \Phi_A \frac{\varepsilon L_{1A} L_2}{H} \lambda_{1A}^2 \lambda_{2A}^2, \tag{1}$$

where ε is the permittivity of the elastomer. Following the deformation of membranes A and B, mass bars move to a new position.

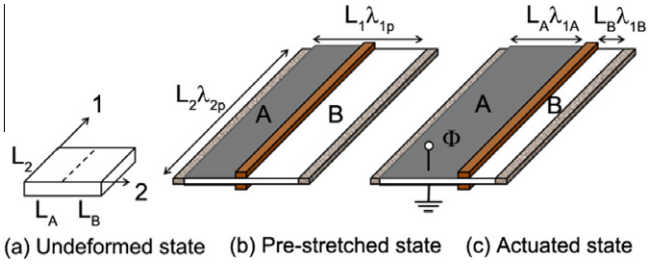

Fig. 1. Schematics of a DE resonator in three states. (a) Undeformed state. The membrane is of length L_1 in the 1-direction, length L_2 in the 2-direction, and thickness H. (b) Pre-stretched state. The membrane is pre-stretched in the 1- and 2-directions and is held by rigid frames. The membrane is of length $L_1\lambda_{1p}$ in the 1-direction and length $L_2\lambda_{2p}$ in the 2-direction. Rigid bars with lumped mass m sandwich the membrane and divide it into membrane A and membrane B. Electrodes are coated on both sides of membrane A. (c) Actuated state. In response to the voltage Φ_A applied on membrane A, membrane A is of length $L_A\lambda_{1A}$ in the 1-direction while membrane B is of length $L_B\lambda_{1B}$ in the 1-direction, and the mass bar moves accordingly.

During actuation, the membranes deform mainly in plane. The total length of the membranes in the 1-direction would remain constant until loss of tension happens in the 1-direction and membranes wrinkle, so that $L_{1A}\lambda_{1A} + L_{1B}\lambda_{1B} = L_1\lambda_{1p}$.

In the spirit of the recent theoretical studies of elastic dielectrics (Dorfmann and Ogden, 2005; McMeeking and Landis, 2005; Suo et al., 2008), one may state the thermodynamics of elastic dielectrics and the kinematics of membranes A and B. Membrane A represents a thermodynamic system of three independent variables λ_{1A}, λ_{2A} and Φ_A, while membrane B of λ_{1B}, λ_{2B} and Φ_B. Both membranes A and B are held at the ambient temperature. Membranes A and B are characterized by the Helmholtz free energy densities $W_A(\lambda_{1A}, \lambda_{2A}, \Phi_A)$ and $W_B(\lambda_{1B}, \lambda_{2B}, \Phi_B)$, which represent their total free energies in the deformed state scaled by the volume of the membranes in an undeformed state. Both systems of membranes A and B evolve with time t. As shown in Fig. 2, membrane A is subject to the voltage Φ_A and tensile forces P_{1A} and P_{2A} in the 1- and 2-directions, while membrane B is only subject to tensile forces P_{1B} and P_{2B}.

When the kinematic variables, λ_{1A} and λ_{2A}, vary slightly, the free-energy density of membrane A changes accordingly, and the tensile forces do work of $P_{1A}L_{1A}\delta\lambda_{1A}$ and $P_{2A}L_2\delta\lambda_{2A}$. When the charge on the electrode varies by δQ_A, the applied voltage does a work of $\Phi_A\delta Q_A$.

During actuation, the inertia force in each material element along the 1-direction is: $-\rho L_2 H x^2(\mathrm{d}^2\lambda_{1A}/\mathrm{d}t^2)$. The total work done by the initial force can be integrated along the length direction: $-\rho L_2 H(\mathrm{d}^2\lambda_{1A}/\mathrm{d}t^2)\delta\lambda_{1A}\int_0^{L_{1A}} x^2\mathrm{d}x$, which gives $(-L_{1A}^3\rho L_2 H/3)(\mathrm{d}^2\lambda_{1A}/\mathrm{d}t^2)\delta\lambda_{1A}$, where ρ denotes the density of the elastomer membrane. The same result can be obtained by the variation of kinetic energy:

$$\begin{aligned} -\delta\left(\int_0^{L_{1A}} \tfrac{1}{2}\rho L_2 H x^2 \left(\tfrac{\mathrm{d}\lambda_{1A}}{\mathrm{d}t}\right)^2 \mathrm{d}x\right) &= -\tfrac{\partial}{\partial t}\left(\int_0^{L_{1A}} \tfrac{1}{2}\rho L_2 H x^2 \left(\tfrac{\mathrm{d}\lambda_{1A}}{\mathrm{d}t}\right)^2 \mathrm{d}x\right)\delta t \\ &= -\rho L_2 H \tfrac{\mathrm{d}^2\lambda_{1A}}{\mathrm{d}t^2}\tfrac{\mathrm{d}\lambda_{1A}}{\mathrm{d}t}\delta t \int_0^{L_{1A}} x^2\mathrm{d}x \\ &= -\tfrac{L_{1A}^3}{3}\rho L_2 H \tfrac{\mathrm{d}^2\lambda_{1A}}{\mathrm{d}t^2}\delta\lambda_{1A}. \end{aligned} \tag{2}$$

For an arbitrary variation of the system, the variation in the free energy of membrane A is equal to the work done jointly by the voltage, the tensile forces and the inertia force,

$$L_{1A}L_2 H\delta W_A = \Phi_A\delta Q_A + P_{1A}L_{1A}\delta\lambda_{1A} + P_{2A}L_2\delta\lambda_{2A} - \frac{L_{1A}^3}{3}\rho L_2 H \times \frac{\mathrm{d}^2\lambda_{1A}}{\mathrm{d}t^2}\delta\lambda_{1A}. \tag{3a}$$

Similarly, for membrane B, with $\Phi_B = 0$, $Q_B = 0$, one has

$$L_{1B}L_2 H\delta W_B = P_{1B}L_{1B}\delta\lambda_{1B} + P_{2B}L_2\delta\lambda_{2B} - \frac{L_{1B}^3}{3}\rho L_2 H\frac{\mathrm{d}^2\lambda_{1B}}{\mathrm{d}t^2}\delta\lambda_{1B} \tag{3b}$$

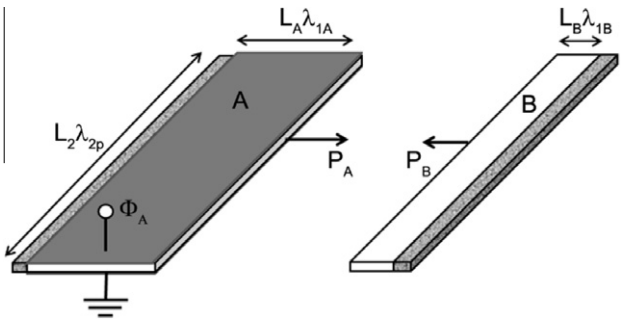

Fig. 2. Schematics of membranes A and B in an actuated state. Membrane A is subject to a voltage Φ_A and a tensile force P_{1A} in the 1-directoin. Membrane B is subjected to a tensile force P_{1B} in the 1-directoin. P_{1A} is equal to P_{1B}

The free-energy density functions W_A and W_B can be decomposed into a static electric energy density and an elastic energy density. The membranes are taken as ideal dielectric elastomers, whose dielectric behaviors are hardly affected by deformation. To capture the strain stiffening effect, we adopt the Gent model to calculate the elastic energy density. Accordingly, the free-energy density functions of membranes A and B take the following form

$$W_A = -\frac{\mu J_{lim}}{2}\log\left(1-\frac{\lambda_{1A}^2+\lambda_{2A}^2+\lambda_{3A}^2-3}{J_{lim}}\right)+\frac{\varepsilon}{2}\left(\frac{\Phi_A}{H}\right)^2\lambda_{1A}^2\lambda_{2A}^2, \quad (4a)$$

$$W_B = -\frac{\mu J_{lim}}{2}\log\left(1-\frac{\lambda_{1B}^2+\lambda_{2B}^2+\lambda_{3B}^2-3}{J_{lim}}\right)+\frac{\varepsilon}{2}\left(\frac{\Phi_B}{H}\right)^2\lambda_{1B}^2\lambda_{2B}^2 \quad (4b)$$

In Eq. (4), the first term on the right hand side describes the elastic energy, with μ being the shear modulus and J_{lim} a constant related to the limiting stretch (Gent, 1996). The material is taken as incompressible, so that the stretches in the thickness direction of the membrane relate to the longitudinal and latitudinal ones by $\lambda_{3A}=1/(\lambda_{1A}\lambda_{2A})$ and $\lambda_{3B}=1/(\lambda_{1B}\lambda_{2B})$. Nominal stresses of membranes A and B are defined as $s_{1A}=P_{1A}/(L_2H)$, $s_{1B}=P_{1B}/(L_2H)$ in the 1-direction, and $s_{2A}=P_{2A}/(L_{1A}H)$, $s_{2B}=P_{2B}/(L_{1B}H)$ in the 2-direction.

Lengths of membranes A and B in the 1-direction are typically much less than those in the 2-direction. The rigid mass bars sandwich the membrane and restrain the deformations of membranes A and B in the 2-direction. As an idealization, we assume that the stretches in the 2-direction of both membranes are the same, i.e. $\lambda_{2A}=\lambda_{2p}$ and $\lambda_{2B}=\lambda_{2p}$, until loss of tension occurs in the 2-direction. Without loss of tension, the nominal stresses of membrane A can be derived from Eqs. (3) and (4) as (see Appendix A):

$$\frac{s_{1A}}{\mu}=\frac{\lambda_{1A}-\lambda_{1A}^{-3}\lambda_{2p}^{-2}}{1-(\lambda_{1A}^2+\lambda_{2p}^2+\lambda_{1A}^{-2}\lambda_{2p}^{-2}-3)/J_{lim}}-\frac{\varepsilon}{\mu}\left(\frac{\Phi_A}{H}\right)^2\lambda_{1A}\lambda_{2p}^2+\frac{L_{1A}^2}{3\mu}\rho\frac{d^2\lambda_{1A}}{dt^2}, \quad (5)$$

$$\frac{s_{2A}}{\mu}=\frac{\lambda_{2p}-\lambda_{2p}^{-3}\lambda_{1A}^{-2}}{1-(\lambda_{1A}^2+\lambda_{2p}^2+\lambda_{1A}^{-2}\lambda_{2p}^{-2}-3)/J_{lim}}-\frac{\varepsilon}{\mu}\left(\frac{\Phi_A}{H}\right)^2\lambda_{2p}\lambda_{1A}^2 \quad (6)$$

Similarly, nominal stresses of membrane B take the form

$$\frac{s_{1B}}{\mu}=\frac{\lambda_{1B}-\lambda_{1B}^{-3}\lambda_{2p}^{-2}}{1-(\lambda_{1B}^2+\lambda_{2p}^2+\lambda_{1B}^{-2}\lambda_{2p}^{-2}-3)/J_{lim}}-\frac{\varepsilon}{\mu}\left(\frac{\Phi_B}{H}\right)^2\lambda_{1B}\lambda_{2p}^2+\frac{L_{1B}^2}{3\mu}\rho\frac{d^2\lambda_{1B}}{dt^2}, \quad (7)$$

$$\frac{s_{2B}}{\mu}=\frac{\lambda_{2p}-\lambda_{2p}^{-3}\lambda_{1B}^{-2}}{1-(\lambda_{1A}^2+\lambda_{2p}^2+\lambda_{1B}^{-2}\lambda_{2p}^{-2}-3)/J_{lim}}-\frac{\varepsilon}{\mu}\left(\frac{\Phi_B}{H}\right)^2\lambda_{2p}\lambda_{1B}^2 \quad (8)$$

when $s_{2A}=0$, membrane A suffers loss of tension and wrinkles in the 2-direction, as reported in the 'pure shear' actuator (Kollosche et al., 2012). After loss of tension, the actuator is under uniaxial tension in the 1-direction, the nominal stresses of membrane A and B take new forms, and Eqs. (5-8) will be rewritten as listed in Appendix B.

During actuation, the actuator is modeled with the consideration on the mass of the rigid bars. The equation of motion is expressed as:

$$P_{1A}-P_{1B}+mL_{1A}\frac{d^2\lambda_{1A}}{dt^2}=0, \quad (9)$$

where m is the lumped mass of the rigid bars sandwiching the membrane.

In an undeformed state, the length of membrane A in the 1-direction is α times that of membrane B, i.e. $L_{1A}=\alpha L_{1B}$. In an actuated state, stretches of membranes A and B in the 1-direction satisfy $\lambda_{1B}=\lambda_{1p}+\alpha(\lambda_{1p}-\lambda_{1A})$. Substituting Eqs. (5-8) into Eq. (9), one obtains the equation of motion as

$$\frac{d^2\lambda_{1A}}{dt^2}+\beta\left(\frac{\lambda_{1A}-\lambda_{1A}^{-3}\lambda_{2A}^{-2}}{1-(\lambda_{1A}^2+\lambda_{2A}^2+\lambda_{1A}^{-2}\lambda_{2A}^{-2}-3)/J_{lim}}-\frac{\varepsilon}{\mu}\left(\frac{\Phi_A}{H}\right)^2\lambda_{1A}\lambda_{2A}^2-\frac{(\lambda_{1p}+\alpha(\lambda_{1p}-\lambda_{1A}))-(\lambda_{1p}+\alpha(\lambda_{1p}-\lambda_{1A}))^{-3}\lambda_{2p}^{-2}}{1-((\lambda_{1p}+\alpha(\lambda_{1p}-\lambda_{1A}))^2+\lambda_{2p}^2+(\lambda_{1p}+\alpha(\lambda_{1p}-\lambda_{1A}))^{-2}\lambda_{2p}^{-2}-3)/J_{lim}}\right)=0 \quad (10)$$

where

$$\beta=1\Big/\left(\frac{L_{1A}m}{\mu HL_2}-\rho\left(\frac{L_{1A}^2}{3\mu}+\alpha\frac{L_{1B}^2}{3\mu}\right)\right) \quad (11)$$

The dimensionless time $t\sqrt{\beta}$ and dimensionless voltage $\Phi/H\sqrt{\varepsilon/\mu}$ will be used in the sequel. When loss of tension occurs on membrane A or B, the membrane may wrinkle. Tensile stresses in membranes A and B should be calculated under uniaxial tension condition (see Appendix B), and Eq. (10) will be revised as suggested therein.

3. Membrane under static voltage

Under the application of static voltage, a DE resonator may reach a state of equilibrium. At that state, stability and failure modes during the actuation may be analyzed by the equilibrium equation. For the resonator, its equilibrium equation can be derived from the equation of motion by neglecting the inertia effect. When a static voltage is applied to membrane A, charges of opposite signs are induced on two electrodes. The electrostatic attraction causes membrane A to contract in thickness and to elongate in the 1-direction with a stretch λ_{1A}. While membrane B shrinks with a stretch λ_{1B}. Mass bars move to a new position. In a state of equilibrium, Eq. (10) is reduced to

$$\frac{\lambda_{1A}-\lambda_{1A}^{-3}\lambda_{2A}^{-2}}{1-(\lambda_{1A}^2+\lambda_{2A}^2+\lambda_{1A}^{-2}\lambda_{2A}^{-2}-3)/J_{lim}}-\frac{\varepsilon}{\mu}\left(\frac{\Phi_A}{H}\right)^2\lambda_{1A}\lambda_{2A}^2-\frac{(\lambda_{1p}+\alpha(\lambda_{1p}-\lambda_{1A}))-(\lambda_{1p}+\alpha(\lambda_{1p}-\lambda_{1A}))^{-3}\lambda_{2p}^{-2}}{1-((\lambda_{1p}+\alpha(\lambda_{1p}-\lambda_{1A}))^2+\lambda_{2p}^2+(\lambda_{1p}+\alpha(\lambda_{1p}-\lambda_{1A}))^{-2}\lambda_{2p}^{-2}-3)/J_{lim}}=0 \quad (12)$$

Consider a simple but a frequently used case where the mass bars are located in the middle of the membrane. In the undeformed state, lengths of membranes A and B in the 1-direction are identical, i.e. $\alpha=1$. Fig. 3a plots the voltage–stretch curve predicted by Eq. (12) with pre-stretches $\lambda_{1p}=2$ and $\lambda_{2p}=3$. Stretch λ_{1A} increases with the applied voltage, while tensile stresses s_{1A} and s_{2A} decrease. In Fig. 3b, the red solid curve characterizes the relation between the nominal stress s_{1A} and the applied voltage, and the black dash curve the relation between the nominal stress s_{2A} and the applied voltage. When s_{2A} diminishes, loss of tension occurs on the 2-direction. Membrane A keeps elongating, while the equilibrium state has to be calculated according to the uniaxial tension case. Similar behavior has been reported in the 'pure shear' actuator (Kollosche et al., 2012). The red dot in Fig. 3a indicates the critical point of $s_{2A}=0$ on the voltage–stretch curve. The blue solid curve represents the voltage–stretch relation under the condition of $\lambda_{2A}=\lambda_{2p}$. The blue dash curve, on the other hand, shows the voltage–stretch relation under uniaxial tension condition, $s_{2A}=0$. The tensile stress s_{1A} declines with the expansion of membrane A. When s_{1A} diminishes, loss of tension happens and the membrane wrinkles in the 1-direction. The mass bar will not move in plane and may fall out of plane since the membrane no longer supports

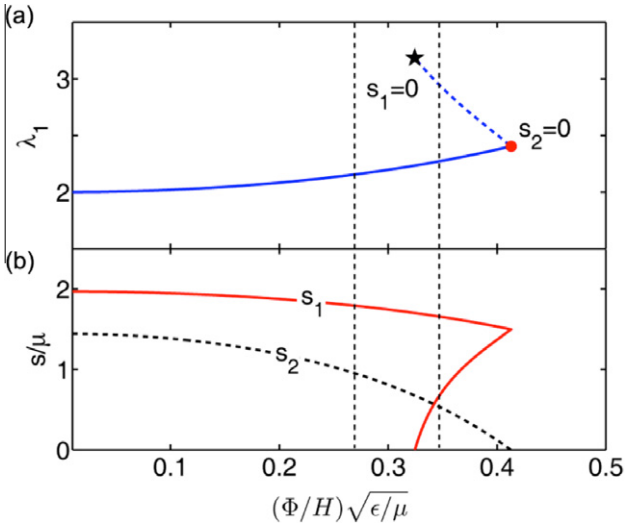

Fig. 3. (a) The equilibrium stretch of membrane A in the 1-direction as a function of the applied voltage. The state of loss tension in the 2-direction, i.e.s_{2A} = 0, is marked by a red dot. The state of loss tension in the 1-direction, i.e. s_{1A} = 0, is marked by a black star. (b) The nominal stresses in membrane A in the 1 and 2-directions as functions of the applied voltage. Red solid curve shows the nominal stress s_{1A} in the 1-direction versus the applied voltage. Black dashed line illustrates the relation in the 2-direction. The parameters are $\alpha = 1$, $\lambda_{1p} = 2$ and $\lambda_{2p} = 3$. (For interpretation of the references to colour in this figure legend, the reader is referred to the web version of this article.)

its weight. The loss of tension in the 1-direction is marked as one failure mode of the resonator. In Fig. 3a, the black star shows the critical point of s_{1A} = 0 on the voltage–stretch curve.

The rising and falling in voltage-stretch curve indicate a snap-through electromechanical instability (Zhao et al., 2007; Zhou et al., 2008; Liu et al., 2011). When the applied voltage reaches the peak (s_{2A} = 0), membrane A will keep expanding at this voltage until loss of tension occurs in the 1-direction (s_{1A} = 0). Consequently, the electromechanical instability will cause the membrane to wrinkle and fail the resonator.

Previous studies reported that pre-stretches strongly affect the behavior of DE actuators (Koh et al., 2011; Kollosche et al., 2012). For different pre-stretches, the voltage-stretch responses of the resonator may vary. Fig. 4a plots the voltage–stretch curves with the same pre-stretch of $\lambda_{1p} = 2$ in the 1-direction, but different pre-stretches, λ_{2p} = 1, 2, 4, in the 2-direction. As discussed before, loss of tension, as well as electromechanical instability, may occur. Similar to Fig. 3a, circles on voltage–stretch curves represent the points that s_{2A} = 0, and stars represent the ones of s_{1A} = 0. Fig. 4a shows that higher pre-stretches in the 1-direction tilt up the voltage–stretch curves and make the resonator more actuable. Larger λ_{2p} delays the loss of tension in the 1-direction and suppresses the electromechanical instability. When $\lambda_{2p} = 4$, loss of tension in the 1-direction is suppressed, and consequently the electromechanical instability is eliminated. The stretch λ_{1A} increases monotonically with the voltage till s_{1A} = 0. Fig. 4b plots the voltage–stretch relation with the same pre-stretch, $\lambda_{2p} = 2$, in the 2-direction but different pre-stretches, λ_{1p} = 1, 2, 4, in the 1-direction. The voltage–stretch curves vary with pre-stretches. When $\lambda_{1p} = 1$, the situation of s_{1A} = 0 occurs prior to the occurrence of s_{2A} = 0.

The effect of mechanical loading paths on the voltage-actuation responses of DE actuators has been reported recently. In the resonator, membrane B exerts a tensile force on membrane A. When the pre-stretches are fixed, loading path of the tensile force can be modified by the parameter α, defined in Section 2. When $\alpha >> 1$, the elongation of membrane A induces significant relaxation of membrane B. Tensile force in the 1-direction declines sharply, which results in high actuation voltage for the resonator. By contrast, when $\alpha << 1$, tensile stress in the 1-direction hardly falls during actuation. In the limit case of $\alpha \to 0$, the voltage-stretch relation recovers the situation of 'pure shear' actuator with constant tensile force (Kollosche et al., 2012). In Fig. 5, the pre-stretches are fixed as $\lambda_{1p} = 2$ and $\lambda_{2p} = 2$. The voltage–stretch curves with different original length ratio of membranes A and B are plotted: (a) α = 0.5, 1, 10; and (b) α = 0.2, 0.0001. Smaller αmakes it easier for the resonator to be actuated with voltage. Voltage–stretch behavior of the resonator becomes insensitive to α when$\alpha \leqslant 0.2$.

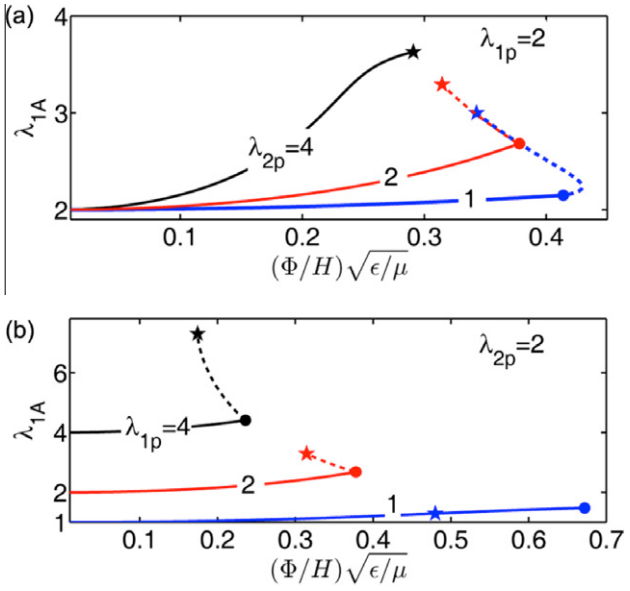

Fig. 4. The equilibrium stretch of membrane A in the 1-direction λ_{1A} as a function of the applied voltage for various pre-stretches. (a) Pre-stretch in the 1-direction is fixed at $\lambda_{1p} = 2$ while pre-stretch in the 2-direction varies (λ_{2p} = 1, 2, and 4). (b) Pre-stretch in the 2-direction is kept at $\lambda_{2p} = 2$ while pre-stretch in the 1-direction varies (λ_{1p} = 1, 2, and 4). The length ratio is taken as α = 1.

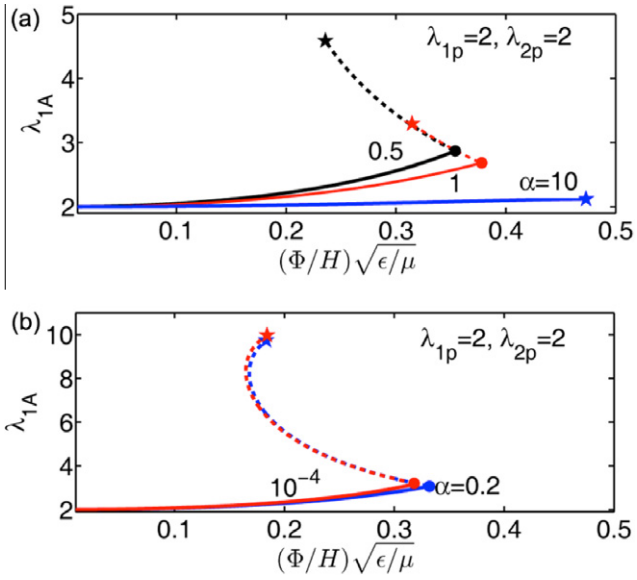

Fig. 5. The equilibrium stretch of membrane A in the 1-direction λ_{1A} versus the applied voltage for various length ratios. (a) α = 0.5, 1, 10; (b) α = 0.2, 0.0001. When the length ratio α is smaller than 0.2, the stretch-voltage curve becomes insensitive to α, and recovers the dead load case of $\alpha \to 0$. The adopted parameters are $\lambda_{1p} = 2$ and $\lambda_{2p} = 3$.

4. Oscillation about the equilibrium state

Following the method adopted in analyzing dielectric elastomers under nonlinear oscillation (Zhu et al., 2010b; Yong et al., 2011), we consider a state of equilibrium of the resonator. When a static voltage Φ_A is applied, membrane A deforms with a stretch λ_{eq} in the 1-direction. The structure is perturbed from this equilibrium state. The stretch of membrane A takes the form

$$\lambda_{1A}(t) = \lambda_{eq} + \Delta(t), \tag{13}$$

where $\Delta(t)$ is the amplitude of perturbation, and is taken to be small.

When the resonator vibrates at high frequencies in a narrow space, loss of tension and wrinkles may happen on the membrane. In this situation, resonator will fail by the collision or the short circuiting between the membranes and the containment of the resonator. We restrain the operation range of the resonator to that without the loss of tension in membranes, and assume that the membranes always satisfy the condition of $\lambda_{2A} = \lambda_{2B} = \lambda_{2p}$. Rewrite Eq. (10) as

$$g(\Phi_A, \lambda_{1A}) + \frac{d^2\lambda_{1A}}{dt^2} = 0, \tag{14}$$

where

$$g(\Phi_A,\lambda_{1A}) = \beta\left(\frac{\lambda_{1A} - \lambda_{1A}^{-3}\lambda_{2p}^{-2}}{1-(\lambda_{1A}^2+\lambda_{2p}^2+\lambda_{1A}^{-2}\lambda_{2p}^{-2}-3)/J_{lim}} - \frac{\varepsilon}{\mu}\left(\frac{\Phi_A}{H}\right)^2\lambda_{1A}\lambda_{2p}^2 - \frac{(\lambda_{1p}+\alpha(\lambda_{1p}-\lambda_{1A}))-(\lambda_{1p}+\alpha(\lambda_{1p}-\lambda_{1A}))^{-3}\lambda_{2p}^{-2}}{1-((\lambda_{1p}+\alpha(\lambda_{1p}-\lambda_{1A}))^2+\lambda_{2p}^2+(\lambda_{1p}+\alpha(\lambda_{1p}-\lambda_{1A}))^{-2}\lambda_{2p}^{-2}-3)/J_{lim}}\right) \tag{15}$$

The function $g(\Phi_A, \lambda_{1A})$ is expanded into a power series around the equilibrium stretch λ_{eq}. To the leading order in Δ, the equation of motion (10) becomes

$$\frac{d^2\Delta}{dt^2} = \tilde{\omega}_0^2\Delta \tag{16}$$

The natural frequency of the resonator takes the form

$$\tilde{\omega}_0^2 = \frac{\partial g(\Phi_A, \lambda_{eq})}{\partial\lambda_{1A}}, \tag{17}$$

where $\tilde{\omega}_0 = \omega 0/\sqrt{\beta}$ is the dimensionless natural frequency. The partial derivative $\partial g(\Phi_A, \lambda_{1A})/\partial\lambda_{1A}$ is evaluated at $\lambda_{1A} = \lambda_{eq}$, and is a constant independent of time. It can be observed from Eq. (10) that the inertia effect of the membrane is negligible when $\frac{L_{1A}m}{HL_2} >> \rho\left(\frac{L_{1A}^2}{3} + \alpha\frac{L_{1B}^2}{3}\right)$.

The natural frequency and the dynamic response of the resonator are determined by the static voltage Φ_A, the pre-stretches λ_{1p} and λ_{2p}, and the coefficients α, β and J_{lim}. For an active tuning resonator, the tunability and the safe range of natural frequency reflect the band width of the devices. The shift in resonant frequency reflects the tuning sensitivity of the devices. Therefore, larger shifts in natural frequency and range are desirable.

Fig. 6 plots that the natural frequency-voltage relation with different pre-stretches. In Fig. 6a, pre-stretch in the 1-direction is kept constant, $\lambda_{1p} = 2$, while the pre-stretches in the 2-direction vary as λ_{2p} = 1, 2, 4. When λ_{2p} = 1, 2, a higher voltage softens the membrane and knocks down the natural frequency of the resonator, until the loss of tension occurs in the 2-direction, as marked by blue and red dots. When $\lambda_{2p} = 4$, a higher voltage first reduces and then enhances the natural frequency of the resonator. This rising and falling voltage-natural frequency curve indicates the stiffening of the resonator under the actuation voltage, which was shown in Fig. 4a, when $\lambda_{1p} = 2$ and $\lambda_{2p} = 4$. The minimum point on the voltage versus natural frequency curve corresponds to the inflection point on the voltage-stretch curve. Loss of tension happens in the 1-direction marked by a black star. It is observed that when $\lambda_{1p} = 2$ and $\lambda_{2p} = 4$, the resonator has a relatively wide tuning range ($\tilde{\omega}_0$ = 1.5–3.3) and a high frequency shift in a narrow range of applied voltages ($\tilde{\Phi}_A$ = 0.23-0.28). In Fig. 6b, the pre-stretch in the 2-direction is kept constant, $\lambda_{2p} = 2$, while the pre-stretches in the 1-direction vary as λ_{1p} = 1, 2, 4. When λ_{1p} = 2, 4, a higher voltage reduces the natural frequency of the resonator, until loss of tension happens in the 2-direction, as marked by red and black dots. When $\lambda_{1p} = 4$, a higher voltage would first reduce and then enhance the natural frequency until loss of tension happens in the 1-direction, as marked by a blue star. When loss of tension happens, the device may become unstable and hard to be tuned by voltage. As discussed before, resonator will fail by the wrinkles of membranes. To avoid failure while tuning, it is essential to control the applied voltage within a safe range. The safe range of the applied voltage is defined as the region from Φ_A = 0 to the voltage level that causes the loss of tension in either 1- or 2-direction. The electrical breakdown is another failure mode in DE-based actuators. In some cases, the electrical breakdown may occur before the loss of tension or the electromechanical instability. Electrical breakdown is affected by material properties and the defects in DE membrane. Following the study of electric breakdown failure of DE actuator (Koh et al., 2011), the maximum applied voltage can be calculated by solving $\Phi/(H\lambda_1\lambda_2) = E_B$ and Eq. (12). We take VHB elastomer as a representative DE material. The material parameters (Wissler and Mazza, 2005a,b; Koh et al., 2011) are set as: electric breakdown field E_B = 160 MV/m, shear modulus μ = 0.068 MPa and permittivity $\varepsilon = 4.5\varepsilon_0$. It is not the aim of the present work to analyze the electrical breakdown failure, here we only take the case of $\lambda_{1p} = 2$ and $\lambda_{2p} = 4$ to exemplify the electric breakdown effect. In that case, the maximum voltage applied to the resonator before electric breakdown is $(\Phi_{max}/H)\sqrt{\varepsilon/\mu} = 0.27$. In Fig. 6a, the red cross on the black curve marks the location of electric breakdown. The operation range of the resonator is defined from zero applied voltage to the electric breakdown limit. Electric breakdown restricted the operation range of the resonator.

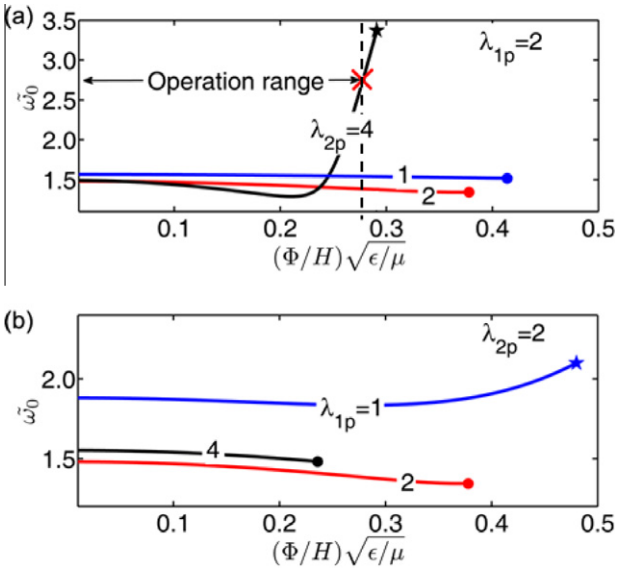

Fig. 6. The natural frequency $\tilde{\omega}_0$ of the resonator versus the applied voltage for various pre-stretches. (a) Pre-stretch in the 1-direction is fixed at $\lambda_{1p} = 2$ while pre-stretch in the 2-direction takes the values of λ_{2p} = 1, 2 or 4. Operation range for λ_{2p} = 4 is marked. (b) Pre-stretch in the 2-direction is fixed at $\lambda_{2p} = 2$ while pre-stretch in the 1-direction takes the values of λ_{1p} = 1, 2 or 4. The length is taken as ratio α = 1.

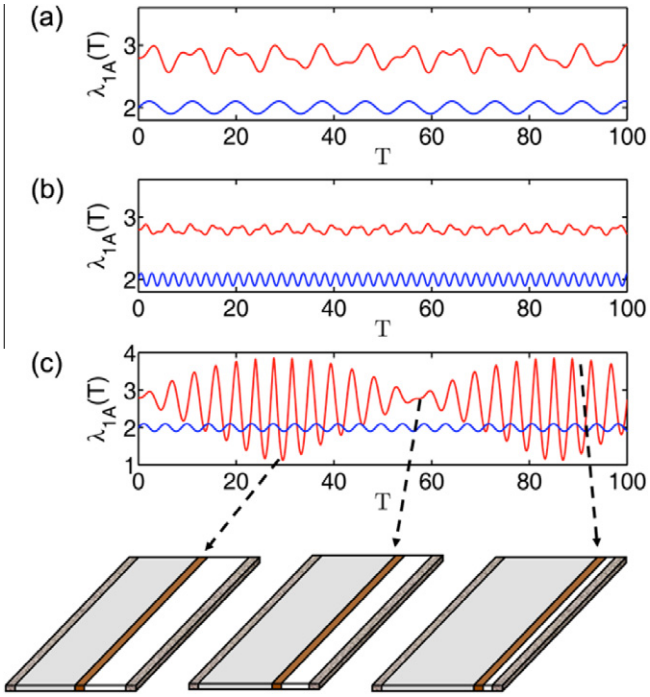

Fig. 7. Nonlinear oscillations of the resonator subject to a sinusoidal voltage for various excitation frequencies. Red curves depict the excitations of the resonator, while blue curves depict the input voltage signals: (a) $\Omega = \tilde{\omega}_0/2$, (b) $\Omega = 2\tilde{\omega}_0$, (c) $\Omega = \tilde{\omega}_0$. The length ratio is taken as $\alpha = 1$, and the pre-stretches are $\lambda_{1p} = 2$ and $\lambda_{2p} = 4$. The sinusoidal voltage is set as $\tilde{\Phi}_{DC} = 0.2$, and $\tilde{\Phi}_{AC}/\tilde{\Phi}_{DC} = 0.05$. (For interpretation of the references to colour in this figure legend, the reader is referred to the web version of this article.)

5. Parametric excitation

When the applied voltage varies with time, the dynamic behavior of the resonator is described by a time dependent stretch $\lambda_{1A}(t)$ of membrane A in the 1-direction. To illustrate the dynamic behavior, we prescribe the voltage signal applied on membrane A as

$$\Phi = \Phi_{DC} + \Phi_{AC}\sin(\Omega t), \tag{18}$$

where Φ_{DC} denotes the static voltage, Φ_{AC} the amplitude of the AC voltage, and Ω the frequency of excitation. The equation of motion, Eq. (10), becomes

$$\frac{d^2\lambda_{1A}}{dT^2} = -\frac{\lambda_{1A} - \lambda_{1A}^{-3}\lambda_{2p}^{-2}}{1-(\lambda_{1A}^2+\lambda_{2p}^2+\lambda_{1A}^{-2}\lambda_{2p}^{-2}-3)/J_{lim}} + \tilde{\Phi}_{DC}^2\left(1+\frac{\Phi_{AC}}{\Phi_{DC}}\sin(\tilde{\Omega}T)\right)^2\lambda_{1A}\lambda_{2p}^2 + \frac{(\lambda_{1p}+\alpha(\lambda_{1p}-\lambda_{1A})) - (\lambda_{1p}+\alpha(\lambda_{1p}-\lambda_{1A}))^{-3}\lambda_{2p}^{-2}}{1-((\lambda_{1p}+\alpha(\lambda_{1p}-\lambda_{1A}))^2+\lambda_{2p}^2+(\lambda_{1p}+\alpha(\lambda_{1p}-\lambda_{1A}))^{-2}\lambda_{2p}^{-2}-3)/J_{lim}} \tag{19}$$

In Eq. (19), $\tilde{\Omega} = \Omega/\sqrt{\beta}$ is the dimensionless excitation frequency, $T = t\sqrt{\beta}$ the dimensionless time, and $\tilde{\Phi}_{DC} = \Phi_{DC}/H\sqrt{\varepsilon/\mu}$ the dimensionless voltage.

DE resonators will undergo parametric excitation when the oscillatory voltage is applied (Nayfeh and Mook, 1979; Jordan and Smith, 1987; Zhu et al., 2010b). The time-dependent stretch can be obtained by solving (19) for a given initial condition. When the static voltage is set as $\tilde{\Phi}_{DC} = 0.2$, the resonator could attain a state of equilibrium with the stretch of membrane A in the 1-direction $\lambda_{eq} = 2.7944$, and with the natural frequency $\tilde{\omega}_0 = 1.424$. This equilibrium state serves as the initial condition in the following numerical simulation. We then apply the alternating voltage. When the numerical solution of $\lambda_{1A}(t)$ attains a steady state of oscillation, the amplitude of oscillation is defined as half of the difference between the maximal and minimal values of $\lambda_{1A}(t)$. Figs. 7a-c exhibit the numerical results of $\lambda_{1A}(t)$ for the same amplitude $\tilde{\Phi}_{DC} = 0.2$ and $\Phi_{AC}/\Phi_{DC} = 0.05$, while different frequencies of excitation, $\tilde{\Omega} = \tilde{\omega}_0/2$, $\tilde{\Omega} = \tilde{\omega}_0$ and $\tilde{\Omega} = 2\tilde{\omega}_0$, are imposed. The resonator oscillates strongly when the frequency of excitation is around the natural frequency of $\tilde{\Omega} = \tilde{\omega}_0$. By applying different DC voltages Φ_{DC}, as discussed in Section 4, natural frequency may be tuned.

6. Discussion

Fig. 8a plots the stroke of the resonator as a function of the frequency of excitation. The length ratio is taken as $\alpha = 1$, and the pre-stretches are $\lambda_{1p} = 2$ and $\lambda_{2p} = 4$. The sinusoidal voltage is set as $\tilde{\Phi}_{DC} = 0.2$, and $\tilde{\Phi}_{AC}/\tilde{\Phi}_{DC} = 0.05$. Resonator vibrates most strongly when the frequency of excitation is around the natural frequency, $\tilde{\Omega} = \tilde{\omega}_0$. The resonator stroke also peaks at $\tilde{\Omega} = \tilde{\omega}_0/2$ and $\tilde{\Omega} = 2\tilde{\omega}_0$ as subharmonic and superharmoinc resonance occur. Resonance at multiple values of the frequency of excitation is common for parametric excitation, and has been reported for a DE resonator (Nayfeh and Mook, 1979; Jordan and Smith, 1987; Zhu et al., 2010b). The Reflex™ HIC Slide Actuator HIC-512 is consisted with 4 segments of the modeled actuator. The blue curve in Fig. 8bshows the Reflex™ HIC Slide Actuator HIC-512 product data (2010) of nonlinear oscillations under various excitation frequencies (Biggs and Hitchcock 2010). For commercial reasons, certain values related to the material, such as the geometries and the excitation voltage signal, have not been reported. To verify our model qualitatively, we set the parameters in our model according to the known experiment data: $\mu = 18$kPa, $m = 25$g, $H = 1$mm, $L_{1A} = 10$mm, $L_2 = 40$ mm, $\varepsilon = 4.16 \times 10^{-12}$ F/m, $\lambda_{1p} = 2$ and $\lambda_{2p} = 4$. The excitation voltage signal as: $\Phi = \Phi_{DC} + \Phi_{AC}\sin(\Omega t)$, with Ω being the frequency of excitation, $\Phi_{DC} = 1$kV, $\Phi_{AC}/\Phi_{DC} = 0.01$. The red curve in Fig. 8b is the simulation result. The overall behavior of nonlinear oscillations are qualitatively comparable. The resonance frequency and resonance stroke (the resonance peak) agrees quite well between the experiment and the modeling results. The widths of the peak, however, are considerably different. The discrepancy between experiment and modeling may result from following reasons: (1) the experiment data reports the resonance

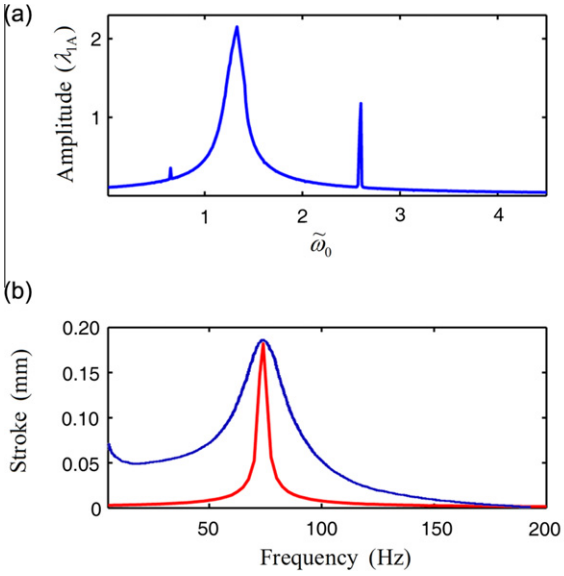

Fig. 8. (a) Excited by a sinusoidal voltage, the resonator resonates at several values of the frequency of excitation. The oscillating amplitude is plotted as a function of the frequency of excitation. (b) The comparison of experiment (blue curve) and simulation (red curve) results. (For interpretation of the references to color in this figure legend, the reader is referred to the web version of this article.)

behavior of the actuator consists of four segments, however the simulation only one segment; (2) the applied voltage signals in experiments may differ from the assumed sinusoidal signals in simulations; and (3) the lack of damping effect in the simulation. In the Reflex™ HIC Slide Actuator HIC-512 (2010) product data, a damping effect after an input voltage pulse is also reported. Since neither viscoelasticity nor current leakage has been included as a dissipation mechanism, the present analysis is unable to demonstrate the damping effect. This discrepancy between theory and experiment and the dissipation mechanisms need to be resolved in future studies.

7. Concluding remarks

A DE membrane resonator with in-plane deformation is analyzed. The equation of motion is described with stretches of the DE membrane. When a static voltage is applied, the resonator may reach a state of equilibrium. Loss of tension, electromechanical instability and electric breakdown may occur and the resonator may fail. The safe range of applied voltages is identified. The pre-stretches and the original length ratios of active and passive membranes strongly affect the behavior of the resonator. We calculate the natural frequency of the resonator with oscillation of small amplitude about the equilibrium state. When the voltage is sinusoidal, the membrane resonates at multiple frequencies of excitation. Dynamic response of the resonator can be modified by actively tuning the natural frequency with static voltage or setting device parameters, such as pre-stretches, length ratios of active and passive membranes, and the lumped mass of rigid bars. This analysis may provide guidelines for the design of tunable DE resonators. Further analysis may include the dissipation mechanisms, such as viscoelasticity and current leakage.

Acknowledgements

This work is supported by the National Natural Science Foundation of China (No. 10832009), the Program for New Century Excellent Talents in University (NCET-08-0480), and the Fundamental Research Funds for the National Universities. Tiefeng Li acknowledges a two-year visit to Harvard University funded by the China Scholarship Council Foundation and by the School of Engineering and Applied Sciences at Harvard.

Appendix A. Equilibrium equations before the loss of tension

Without the loss of tension, the nominal stresses of membrane A in the 1-direction can be derived from Eqs. (3) and (4). From Eq. (3a), one has:

$$\frac{P_{1A}\delta\lambda_{1A}}{L_2H} = \delta W_A - \frac{\Phi_A\delta Q_A + P_{2A}L_2\delta\lambda_{2A} - \frac{L_{1A}^3}{3}\rho L_2 H\frac{d^2\lambda_{1A}}{dt^2}\delta\lambda_{1A}}{L_{1A}L_2H} \tag{A.1}$$

Substitute Eq. (4a) into (A.1) and manipulate, one arrives at:

$$\frac{P_{1A}\delta\lambda_{1A}}{L_2H} = \delta\left(-\frac{\mu J_{lim}}{2}log\left(1-\frac{\lambda_{1A}^2+\lambda_{2A}^2+\lambda_{3A}^2-3}{J_{lim}}\right)\right) + \delta\left(\frac{\varepsilon}{2}\left(\frac{\Phi_A}{H}\right)^2\lambda_{1A}^2\lambda_{2A}^2\right) - \frac{\Phi_A\left(2\Phi_A\frac{\varepsilon L_{1A}L_2}{H}\lambda_{2A}^2\lambda_{1A}\delta\lambda_{1A}\right) - \frac{L_{1A}^3}{3}\rho L_2H\frac{d^2\lambda_{1A}}{dt^2}\delta\lambda_{1A}}{L_{1A}L_2H} \tag{A.2}$$

After algebraic manipulation, the right hand side is reduced to:

$$\frac{P_{1A}\delta\lambda_{1A}}{L_2H} = \frac{\lambda_{1A}-\lambda_{1A}^{-3}\lambda_{2A}^{-2}}{1-(\lambda_{1A}^2+\lambda_{2A}^2+\lambda_{1A}^{-2}\lambda_{2A}^{-2}-3)/J_{lim}}\mu\delta\lambda_{1A} - \varepsilon\left(\frac{\Phi_A}{H}\right)^2\lambda_{1A}\lambda_{2A}^2\delta\lambda_{1A} + \frac{L_{1A}^2}{3}\rho\frac{d^2\lambda_{1A}}{dt^2}\delta\lambda_{1A} \tag{A.3}$$

Observe that $s_{1A} = P_{1A}/(L_2H)$ from the definition of nominal stress, one further has:

$$\frac{s_{1A}}{\mu} = \frac{\lambda_{1A}-\lambda_{1A}^{-3}\lambda_{2p}^{-2}}{1-(\lambda_{1A}^2+\lambda_{2A}^2+\lambda_{1A}^{-2}\lambda_{2A}^{-2}-3)/J_{lim}} - \frac{\varepsilon}{\mu}\left(\frac{\Phi_A}{H}\right)^2\lambda_{1A}\lambda_{2A}^2 + \frac{L_{1A}^2}{3\mu}\rho\frac{d^2\lambda_{1A}}{dt^2} \tag{A.4}$$

The nominal stresses of membrane A in the 2-direction can be derived analogously.

Appendix B. Membrane under uniaxial tension

When membrane A or B is under uniaxial tension, membrane wrinkles in the 2-direction. The stretches in the 2-direction of membrane A or B would no longer satisfy the condition of $\lambda_{2A} = \lambda_{2p}$ or $\lambda_{2B} = \lambda_{2p}$. If the compressive stress in the 2-direction is neglected, i.e. $s_{2A} = 0$, Eqs. (4) and (5) are replaced by

$$\frac{s_{1A}}{\mu} = \frac{\lambda_{1A}-\lambda_{1A}^{-3}\lambda_{2A}^{-2}}{1-(\lambda_{1A}^2+\lambda_{2A}^2+\lambda_{1A}^{-2}\lambda_{2A}^{-2}-3)/J_{lim}} - \frac{\varepsilon}{\mu}\left(\frac{\Phi_A}{H}\right)^2\lambda_{1A}\lambda_{2A}^2 + \frac{L_{1A}^2}{3\mu}\rho\frac{d^2\lambda_{1A}}{dt^2} \tag{B.1}$$

$$\frac{\lambda_{2A}-\lambda_{2A}^{-3}\lambda_{1A}^{-2}}{1-(\lambda_{1A}^2+\lambda_{2A}^2+\lambda_{1A}^{-2}\lambda_{2A}^{-2}-3)/J_{\lim}} - \frac{\varepsilon}{\mu}\left(\frac{\Phi_A}{H}\right)^2\lambda_{2A}\lambda_{1A}^2 = 0 \tag{B.2}$$

Similarly, Eqs. (6) and (7) should be replaced by

$$\frac{s_{1B}}{\mu} = \frac{\lambda_{1B}-\lambda_{1B}^{-3}\lambda_{2B}^{-2}}{1-(\lambda_{1B}^2+\lambda_{2B}^2+\lambda_{1B}^{-2}\lambda_{2B}^{-2}-3)/J_{\lim}} - \frac{\varepsilon}{\mu}\left(\frac{\Phi_B}{H}\right)^2\lambda_{1B}\lambda_{2B}^2 + \frac{L_{1B}^2}{3\mu}\rho\frac{d^2\lambda_{1B}}{dt^2}, \tag{B.3}$$

$$\frac{\lambda_{2B}-\lambda_{2B}^{-3}\lambda_{1B}^{-2}}{1-(\lambda_{1A}^2+\lambda_{2B}^2+\lambda_{1B}^{-2}\lambda_{2B}^{-2}-3)/J_{\lim}} - \frac{\varepsilon}{\mu}\left(\frac{\Phi_B}{H}\right)^2\lambda_{2B}\lambda_{1B}^2 = 0 \tag{B.4}$$

when $s_{2B} = 0$.

References

Anderson, I.A., Hale, T., Gisby, T., Inamura, T., McKay, T., O'Brien, B., Walbran, S., Calius, E.P., 2010. A thin membrane artificial muscle rotary motor. Appl. Phys. A-Mater. 98, 75–83.

Bar-Cohen, Y., 2002. Electroactive polymers as artificial muscles: a review. J. Spacecraft. Rockets 39, 822–827.

Biggs, S.J., Hitchcock, R.N., 2010. Artificial muscle actuators for haptic displays: system design to match the dynamics and tactile sensitivity of the human fingerpad. Proc. SPIE 7642, 76420I.

Bonwit, N., Heim, J., Rosenthal, M., Duncheon, C., Beavers, A., 2006. Design of commercial applications of EPAM technology. Proc. SPIE. 6168, 39–48.

Carpi, F., Rossi, D.D., Kornbluh, R., Pelrine, R., Sommer-Larsen, P., 2008. Dielectric Elastomers as Electromechanical Transducers: Fundamentals, Materials, Devices, Models and Applications of an Emerging Electroactive Polymer Technology. Elsevier, UK.

Carpi, F., Bauer, S., De Rossi, D., 2010. Stretching dielectric elastomer performance. Science 330, 1759–1761.

Dorfmann, A., Ogden, R.W., 2005. Nonlinear electroelasticity. Acta Mech. 174, 167–183.

Dubois, P., Rosset, S., Niklaus, M., Dadras, M., Shea, H., 2008. Voltage control of the resonance frequency of dielectric electroactive polymer (DEAP) membranes. J. Microelectromech. Syst. 17, 1072–1081.

Feng, C., Jiang, L.Y., Lau, W.M., 2011. Dynamic characteristics of a dielectric elastomer-based microbeam resonator with small vibration amplitude. J. Micromech. Microeng. 21, 095002.

Fox, J.W., 2007. Electromechanical Characterization of the Static and Dynamic Response of Dielectric Elastomer Membranes, Master Thesis, Virginia Polytechnic Institute and State University.

Fox, J.W., Goulbourne, N.C., 2008. On the dynamic electromechanical loading of dielectric elastomer membranes. J. Mech. Phys. Solids 56, 2669–2686.

Fox, J.W., Goulbourne, N.C., 2009. Electric field induced surface transformations and experimental dynamic characteristics of dielectric elastomer membranes. J. Mech. Phys. Solids 57, 1417–1435.

Gent, A.N., 1996. A new constitutive relation for rubber. Rubber Chem. Technol. 69, 59–61.
Jordan, D.W., Smith, P., 1987. Nonlinear Ordinary Differential Equations. Clarendon Press, Oxford.
Keplinger, C., Li, T.F., Baumgartner, R., Bauer, S., Suo, Z.G., 2011. Harnessing snap-through instability in soft dielectrics to achieve giant voltage-triggered deformation. Soft Matter 8, 285–288.
Koh, S.J.A., Li, T.F., Zhou, J.X., Zhao, X.H., Hong, W., Zhu, J., Suo, Z.G., 2011. Mechanisms of large actuation strain in dielectric elastomers. J. Polym. Sci. Pol. Phys. 49, 504–515.
Kollosche, M., Zhu, J., Suo, Z.G., Kofod, G., 2012. Complex interplay of nonlinear processes in dielectric elastomers. Phys. Rev. E 85, 051801.
Li T. F., Keplinger, C., Baumgartner, R., Bauer, S., Yang, W., Suo, Z.G., submitted for publication. Giant voltage-induced deformation in dielectric elastomers near the verge of snap-through instability.
Liu, L.W., Liu, Y.J., Li, B., Yang, K., Li, T.F., Leng, J.S., 2011. Thermo-electro-mechanical instability of dielectric elastomers. Smart. Mater. Struct. 20, 075004.
Mckay, T., O'Brien, B., Calius, E., Anderson, I., 2010. An integrated, self-priming dielectric elastomer generator. Appl. Phys. Lett. 97 (6), 062911.
McMeeking, R.M., Landis, C.M., 2005. Electrostatic forces and stored energy for deformable dielectric materials. J. Appl. Mech-T. ASME. 72, 581–590.
Mockensturm, E.M., Goulbourne, N.C., 2006. Dynamic response of dielectric elastomers. Int. J. Non-Linear. Mech. 41, 388–395.
Nayfeh, A.H., Mook, D.T., 1979. Nonlinear Oscillation. Wiley, New York.
Pelrine, R., Kornbluh, R., Pei, Q.B., Joseph, J., 2000. High-speed electrically actuated elastomers with strain greater than 100%. Science 287, 836–839.
Plante, J.S., Dubowsky, S., 2006. Large-scale failure modes of dielectric elastomer actuators. Int. J. Solids. Struct. 43, 7727–7751.
Plante, J.S., Dubowsky, S., 2007. On the performance mechanisms of dielectric elastomer actuators. Sensors and Actuators A 137, 96–109.
Reflex™ HIC Slide Actuator HIC-512 Product data, 2010. (AMI Website: www.artificialmuscle.com).
Suo, Z.G., Zhao, X.H., Greene, W.H., 2008. A nonlinear field theory of deformable dielectrics. J. Mech. Phys. Solids. 56, 467–486.
Wissler, M., Mazza, E., 2005a. Modeling of a pre-strained circular actuator made of dielectric elastomers. Sensors and Actuators A 120, 184–192.
Wissler, M., Mazza, E., 2005b. Modeling and simulation of dielectric elastomer actuators. Smart. Mater. Struct. 14, 1396–1402.
Xia, J.Q., Ying, Y.R., Foulger, S.H., 2005. Electric-field-induced rejection wavelength tuning of photonic bandgap composites. Adv. Mater. 17, 2463–2467.
Yong, H.D., He, X.Z., Zhou, Y.H., 2011. Dynamics of a thick-walled dielectric elastomer spherical shell. Int. J. Eng. Sci. 49, 792–800.
Zhao, X.H., Hong, W., Suo, Z.G., 2007. Electromechanical coexistent states and hysteresis in dielectric elastomers. Phys Rev B 76, 134113.
Zhou, J.X., Hong, W., Zhao, X.H., Zhang, Z.Q., Suo, Z.G., 2008. Propagation of instability in dielectric elastomers. Int. J. Solids. Struct. 45, 3739–3750.
Zhu, J., Cai, S.Q., Suo, Z.G., 2010a. Nonlinear oscillation of a dielectric elastomer balloon. Polym. Int. 59, 378–383.
Zhu, J., Cai, S.Q., Suo, Z.G., 2010b. Resonant behavior of a membrane of a dielectric elastomer. Int. J. Solids. Struct. 47, 3254–3262.